HardwareX 10 (2021) e00222

Contents lists available at ScienceDirect

HardwareX

journal homepage: www.elsevier.com/locate/ohx

PlateFlo – A software-controllable plate-scale perfusion system for culture of adherent cells

Robert Pazdzior, Stefan Kubicek *

CeMM Research Center for Molecular Medicine of the Austrian Academy of Sciences, Vienna, Austria

ARTICLE INFO

Article history:
Received 6 May 2021
Received in revised form 23 July 2021
Accepted 5 August 2021

Keywords:
Adherent
Perfusion
Millifluidic
Microplate
Cell culture
Automation

ABSTRACT

Here we present a versatile system for milliliter-scale perfusion culture of adherent cells that can be built using basic tools, based on a readily available one-well culture plate (84 cm^2 culture area). Media composition and flow paths can be programmatically controlled via USB serial interface using the FETbox hardware controller and associated PlateFlo Python package. The FETbox can control up to five high current 12 V devices such as common pinch valves, solenoids, and DC motor peristaltic pumps. It was designed to be easily customized with built-in accommodation for additional electronic components (e.g. analog sensors and input), use of the ubiquitous Arduino Nano platform, and easily expanded serial communication protocol. Multiple FETboxes can be used in parallel for additional devices. Applications of the PlateFlo system include perfusion culture of laboratory experiments requiring large cell numbers including genome-scale genetic screens and proteomics, as well as novel perfusion schemes including dynamic media conditions and sequential cell culture.

Specifications table

Hardware name	*PlateFlo plate-scale perfusion system*
Subject area	• Biological Sciences (e.g. Microbiology and Biochemistry)
Hardware type	• Biological sample handling and preparation
Open Source License	*Software - GNU General Public License (GPL) v3;* *Hardware - CERN Open Hardware License, Weakly Reciprocal (OHL-W) v1.2*
Cost of Hardware	*Hardware: 350 EUR** *Consumables: < 10 EUR/plate*
Source File Repository	OSF - https://doi.org/10.17605/OSF.IO/PYJCH

*Minimum of two additional individually controllable peristaltic pumps, and associated tubing/fittings are required.

Abbreviations: BOM, bill of materials; CFD, computational fluid dynamics; DMEM, Dulbecco's modified Eagle's medium; EUR, Euro; FDM, fused deposition modelling; hIPSC, human induced pluripotent stem cell; MCU, microcontroller unit; MOSFET, metal oxide semiconductor field effect transistor; PBS, phosphate-buffered saline; PCB, printed circuit board; PWM, pulse width modulation.

* Corresponding author.
E-mail address: SKubicek@cemm.oeaw.ac.at (S. Kubicek).

https://doi.org/10.1016/j.ohx.2021.e00222
2468-0672/

Hardware in context

Most in vitro tissue culture models used in biological research, be it immortalized cell lines or primary tissue, are cultured in traditional petri dishes or multi-well plates under a static pool of nutrient medium. Cells in static culture are subjected to unphysiological buildup of secreted factors and waste products while simultaneously depleting glucose, amino acids, and other nutrients from the medium. This gradual decline/accumulation is punctuated by a sharp reversal in concentration trends when the nutrient medium is periodically renewed in bulk during regular cell maintenance [1]. This creates unintended temporal heterogeneity in the extracellular environment that could be a confounding factor in some biological systems. Static culture also lacks the mechanical stimulation provided by fluid shear forces along vesicles and within the interstitial in vivo, a key factor in the differentiation of endothelial cells [2] and osteoclasts [3], for example. One way to overcome these shortcomings is to continuously perfuse fresh or partially recirculated nutrient medium through the culture vessel [4,5]. Different technical solutions for perfusion cell culture have been implemented (Table 1).

Stirred-tank bioreactors are commonly employed in perfusion culture, particularly in industry [6]. These are culture vessels in which cells are kept in suspension by an impellor and medium is supplied and drawn from the tank to maintain nutrient concentration, pH, and other process factors. This style of perfusion device is effective at maintaining high cell density and is thus favored in production, particularly of recombinant proteins such as antibodies. Commercial laboratory-scale solutions also exist, for example disposable spinner flasks that are available in different sizes with sidearms for inlet/outlet connection. Many cell types are anchorage-dependent (adherent), however, and are not viable in suspension [7] on their own. In order to culture these cells in suspension, suspended particles are utilized to provide a suitable surface for attachment and growth [8]. These so-called microcarriers have proven effective in stirred reactors, particularly for example, with mesenchymal stem cells, and can be tuned in numerous ways including size, shape, and porosity.

Hollow fiber bioreactors are well-suited to adherent cell culture [9]. They consist of many semi-porous capillaries through which nutrient media is circulated and a surrounding compartment in which cells are seeded and grow [10], often in the form of a single-use cartridges in commercial solutions (e.g. FiberCell Systems Inc., Cellab GmbH, and Terumo BCT Inc.). Small molecules and dissolved gas perfuse through the porous tubing in both directions, providing nutrients to- and removing waste from cells adhering to the tubing within the outer compartment. Hundreds, even thousands, of capillary tubes can fit in a single cartridge, thus, an extremely large growth area is possible in a relatively small footprint. Cells grow to very high confluency and secreted protein products and extracellular vesicles can be continuously collected downstream and concentrated, thus making hollow fiber bioreactors highly effective in production applications. The main downside, as with most commercial solutions, is the upfront cost for ready-built systems as well as the recurring price of consumable single-use bioreactor cartridges. Cells must be harvested, e.g. trypsinized, in order to perform microscopy thus strongly perturbing the system. Because of the compartmentalized nature of the nutrient media flow path, cells are isolated from shear stress – which may be desirable in some applications but is less physiological than direct perfusion.

Microfluidic devices offer near infinite diversity in design, limited only by the imagination and fabrication skill of the creator, and can be tailored to fit the application or biological question at hand [11]. Microfluidic devices can be fabricated by a wide variety of methods, most of which require specialized equipment and skills such as photolithography [12], CNC milling [13], or laser micromaching [14]. The alternative, commercial solutions, whether it be custom or off-the-shelf can be cost-prohibitive, depending on complexity and specialization. The small scale of microfluidic chips permits precise real-time control of flow parameters and composition while avoiding dilution of secreted factors important for e.g. hormone secretion assays. With this small scale comes some limitations, however; pumping and directing flow at nanoliter flow rates, often with pneumatic systems, can be more complex to setup/control. Biological material generation can also be a limiting factor for downstream readouts such as proteomics and genome-scale genetic screening.

In the broad class of bioreactors termed here ‘perfused scaffold chamber’ reactors, cells or tissue models are embedded within a permeable matrix that allows media to flow directly through the entire construct. The oscillating chamber bioreactor, patented by Moretti [15,16], utilizes a similar concept but takes a unique approach in implementing it. Instead of mechanically pumping media through the chamber with e.g. a peristaltic pump, gas-permeable semi-circular reservoir tubing containing nutrient medium on either side of the chamber alternatingly perfuses the interstitial space by gravity; this is achieved by rotating the entire chamber back and forth along the axis perpendicular to the plane of the tubing path [17]. In these systems the chamber can be constructed with a transparent window for optical readout and sensors and electrodes integrated for monitoring or stimulation. Interstitial perfusion allows for thorough exchange with the perfusion medium and full compatibility with three-dimensional tissue models. The obligatory support matrix, while often beneficial for 3D tissue models, adds complexity to both setup and harvest. Common matrix supports, such a Matrigel, can also complicate downstream proteomic preparation [18] or negatively impact proteomic results if not considered.

Perfused well bioreactors are also a diverse class of devices, but many assume a roughly microplate footprint with several culture chambers therein. Some examples are given in Table 1 that range in scale from 96- to 12-well formats. These are constructed using a variety of techniques including (micro)machining, silicon wafer etching, and PDMS casting. These smaller wells are well suited to experiments requiring multiple treatments or conditions, especially Domansky et al’s multi-well plate where each well has an independent reservoir and medium is pumped through the 14.9 mm culture scaffolds using pneumatic diaphragm micropumps [19]. Pasini et al, in contrast, use serially perfused chambers in a 12-well format machined from PMMA (acrylic) in combination with glass coverslip culture surfaces for more traditional 2D cell culture [20].

Table 1
A general overview of comparable perfusion culture approaches.

Bioreactor Type	Description	Examples	Comments		
Perfused Plate	Modified commercial rectangular culture plates or petri dishes with treated culture surface over which media flows	This work		Cost Scale Flow Rate Complexity Availability Adherent/ Suspension 2D/3D	$ +++ 84 cm^2 culture area 10–25 mL 0.1–10 mL/min ++ Open-source Adherent 2D
Perfused Well	Diverse custom fabricated multi-well constructions. Some incorporating pumping directly in each well or utilizing hydrostatic (gravity) feeding.	[40–42], e.g. Corning MicroDEN	Complexity is primarily driven by (micro)fabrication requirements.	Cost Scale Flow Rate Complexity Availability Adherent/ Suspension 2D/3D	$$ + μL/min +++ Publication, Commercial Adherent or matrix embedded 2D
Perfused Scaffold Chamber	Cells or tissue contained in a perfusable cartridge-like scaffold/matrix	[43–46]	Diverse class of devices. Scaffold size, composition, and topology are highly tunable.	Cost Scale Flow Rate Complexity Availability Adherent/ Suspension 2D/3D	$$ ++ Diverse. μL/min - mL/min +++ Publication Adherent/embedded 3D
Hollow-Fiber Bioreactor	Waste/nutrient exchange via semi-porous capillary tubing and cells grown in extra-capillary space. The massive number of capillaries that can be contained inside a culture chamber enables extremely high culture density.	[8,10,47]	Diverse commercial solutions due to use in part to widespread use in the production of biologicals. Lab-scale solutions also available. Capillary fouling is must be considered. See text for examples. See [48] for a summary of production technologies including hollow-fiber bioreactors.	Cost Scale Flow Rate Complexity Availability Adherent/ Suspension 2D/3D	$$$-$$$$ ++ - ++++ Up to 200 cm^2/mL Diverse ++ Commercial Both 2D
Oscillating Chamber Bioreactor	Sensor-equipped, optically transparent construct chamber perfused by oscillating motion of medium through connected semi-circular gas permeable tubing.	[38,39]	All-in-one device allows electrical stimulation, electrical sensor integration, and optical readouts.	Cost Scale Flow Rate Complexity Availability Adherent/ Suspension 2D/3D	$$$ ++ ø 12 mm × h 3 mm, 10 mL medium, per chamber. 100 μm/s linear equivalent ++++ Publication, Commercialized Both 3D

(*continued on next page*)

Table 1 (*continued*)

Bioreactor Type	Description	Examples	Comments		
Stirred Tank Bioreactor	An impellor agitates the culture medium, preventing cells from sedimenting while maximizing waste removal and nutrient delivery by homogenizing the medium.	[48,49], e.g. Corning Spinner Flasks	Basic in principle, but endlessly customizable and extremely scalable. Sensors can be easily integrated, impellor design optimized, and diverse microcarriers utilized. Continuous perfusion is complicated by the need for filtration or other solutions to prevent aspiration of suspended cells. Fed-batch is a simplified alternative to continuous feeding/perfusion.	Cost Scale Flow Rate Complexity Availability Adherent/ Suspension 2D/3D	$ - $$$$ + - ++++ mL – kL μL/min – L/s Diverse Diverse Suspension, adherent on micro-carriers, adherent as spheroids 3D

The "PlateFlo" system presented here is a flexible, low cost, solution for laboratory-scale perfusion of adherent cells. It can be built using only basic tools and the modular nature of the design allows for substitution of main components to better suit specific applications if need be. The perfusion plate design utilizes a modified off-the-shelf culture plate rather than a custom-fabricated culture chamber. This lidded, one-well, rectangular microplate can be loaded with cells, pre-treated, imaged, etc., as a typical culture plate independently of the fluidic components of the system. This improves sterile handling, allows for microscopy-based readouts, and is compatible with diverse cell harvesting methods – e.g. cell scraping, trypsinization, or in-plate lysis. Biological material can be generated in sufficient quantity from a single plate for unbiased multi-omics analysis including proteomics and various sequencing technologies. The electronic components of the system are intended to interface via USB with a control computer where dynamic perfusion programs can be created using the plateflo Python library, or any serial interface capable software such as LabVIEW.

The most comparable commercial alternative to the PlateFlo system is the Corning MicroDEN perfusion platform. Similar to the device presented here, media is pumped across a tissue culture surface continuously using peristaltic pumps. A key difference is the closed nature of the perfusion chamber, and closed loop recirculating flow approach which uses a single pump for each chamber. Each recirculating flow path has a 13 mL volume and advertised yield of six million cells each and is marketed for production of dendritic cells. At the time of writing, this system was listed for $18,430, and the single-use perfusion chamber/reservoir combo unit was listed at $1930 per pair. The MicroDEN platform is purpose-built for a specific application, however, thus lacks the versatility and flexibility of the PlateFlo system; with the system described here media can be recirculated (closed loop) or continuously exchanged (open loop), selected from multiple reservoirs using one or more valves, the pumps controlled dynamically, and more. With the PlateFlo system we provide as many tools as possible to adapt it to suite a wide range of experimental setups.

Hardware description

The PlateFlo system consists of three main components: (1) the perfusion plate and associated fluidics for cell culture, (2) the FETbox hardware controller for high-current device control (e.g. valves, DC pumps), and (3) the plateflo Python package for programmatic control over (1) and (2). These components are presented as a toolbox with which it is possible to build plate-scale perfusion systems ranging in complexity from a single plate, single reservoir, constant flow rate setup to e.g. a sequential culture system chaining multiple cell lines in series, dosing glucose, drugs, or different nutrient medium on a predefined schedule.

Perfusion plate

The perfusion culture chamber is a modified Nunc OmniTray one-well plate (Fig. 1). The culture area of a Nunc OmniTray plate is 84 cm^2, for reference, this is approximately 50% greater than that of a typical 10 cm petri dish (55 cm^2). Nutrient medium is pumped in one side and out the other, flowing nearly uniformly across the culture surface. Only modifications to the lid are necessary, therefore it can be built, sterilized, and otherwise handled independently of the base. This permits hot swapping of the plate base for e.g. microscopy, additional biological replicates, etc., without having to disassemble and re-sterilize the associated fluidics. Standard 200 μL (P200) pipette tips are repurposed for the nozzles and are inserted through drilled holes in the plate lid with tubing press fit into the tapered section of the pipette tip. A modified lid can be reused several times with replacement of the nozzles as necessary to avoid cross-contamination.

Two independently controllable peristaltic pumps are required to pump fresh media into the plate and remove the effluent simultaneously - one for the inlet nozzle and one for the pair of outlet nozzles. Multi-channel peristaltic pumps can be used to run multiple plates in parallel. The need for two peristaltic pumps introduces a technical challenge, however; if the inlet and outlet flow rates are not absolutely identical there will be a net movement of media into or out of the perfusion plate, potentially overflowing or running dry; for example, at a flow rate of 120 μL/min, just a 1% difference between the inlet and outlet flow rates will result in a plate volume change of greater than 5 mL over the course of 72 h (~50% of the OmniTray working volume used here). To avoid the added cost and complexity of closed-loop sub-milliliter flow metering, or constant pump recalibration and validation, for example, a 'skimming' system was implemented for plate volume regulation.

An additional independent outlet nozzle, the skimmer nozzle, is set at the desired fluid height using a 3D printed clamping mechanism and height blocks. The main outlet pump is run marginally slower than the inlet to ensure a small net positive influx of media. The exact flow rate delta should be a safe margin, determined by characterizing the flow rate accuracy of the specific pumps and cassette tubing chosen. An inexpensive peristaltic pump or aspirator is used to remove the small excess media as it reaches the skimmer. This eliminates the need for expensive, complex, and potentially difficult to clean microflow meters and closed-loop pump control.

FETbox hardware controller

The FETbox hardware controller enables USB serial controlled switching of up to five high-current 12 V devices such as pinch valves, solenoids, and DC motor peristaltic pumps (Fig. 2A). Some of these outputs are intended to drive inexpensive skimmer pumps or aspirator solenoid valves. The remaining outputs or additional FETboxes can be used for fluid path control in the system via pinch valves – e.g. switching between media reservoirs, recirculating media, or redirecting effluent to a sampling system.

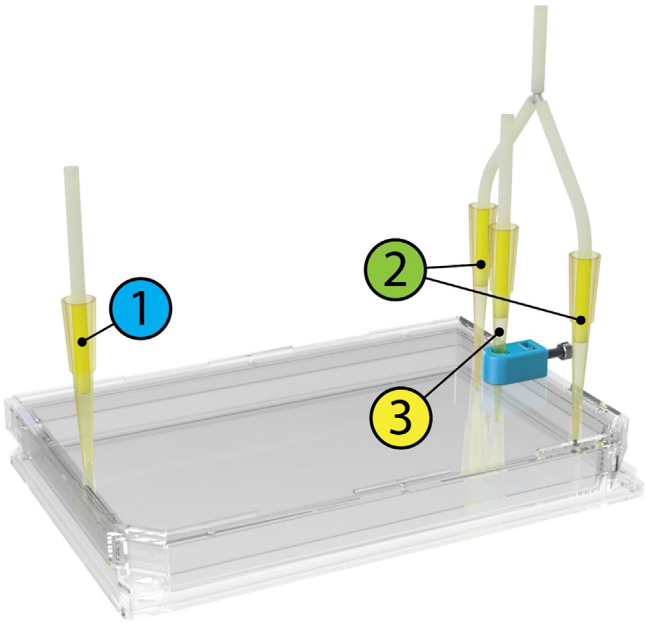

Fig. 1. PlateFlo Perfusion Plate. A Nunc OmniTray base with lid modified with 1) one inlet nozzle, 2) two outlet nozzles, and 3) a height-adjustable skimmer nozzle with 3D printed clamping mechanism.

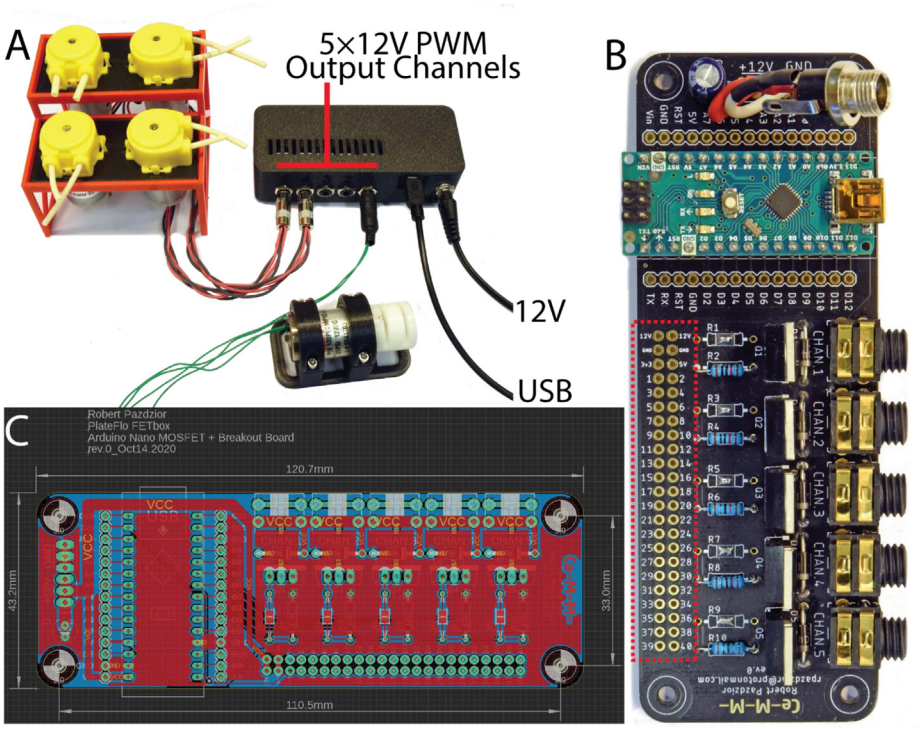

Fig. 2. FETbox Hardware Controller. A) Example application of the FETbox, controlling a bank of inexpensive 12 V peristaltic pumps for four skimmer channels and a solenoid pinch valve. B) Assembled FETbox PCB. Dotted red box indicates unconnected solder pads for user customizability and expansion. C) FETbox board overview in EAGLE CAD software, red denotes top copper layer, blue the bottom copper layer as viewed through the top. (For interpretation of the references to colour in this figure legend, the reader is referred to the web version of this article.)

Through-hole devices were used exclusively, avoiding surface mount devices (SMDs), in the design of the FETbox circuit board to make board assembly accessible to soldering novices. It is built around the ubiquitous open-source Arduino Nano development board and ATmega 328P micro controller unit (MCU), with all board pins broken out onto the PCB for user customizability (Fig. 2B, C). There is also a 2.54 mm (0.1″) 2 × 20 grid of unconnected through-holes along with + 12/+5/+ 3.3 V and GND connections for mounting of additional connectors and components (Fig. 2B, red box). To further simplify customization of the board, the plateflo Python package's fetbox module includes methods to read and set all analog/digital pins on the Arduino Nano via USB serial. Custom serial commands can be added easily to the Arduino firmware for e.g. querying digital sensors or additional functionality (see "Firmware Modification" in the online documentation). At the default baud rate of 115,200 bits/sec, approximately 50–60 commands/queries can be sent per second for e.g. data logging purposes.

Each FETbox can supply + 12 V up to a total of 4.5 A through the five PWM-capable MOSFET-switched outputs, with each individual device drawing no more than 3 A. In order to minimize the BOM component count, +5 V is supplied from the Arduino's onboard regulator and limited to ~ 350 mA for peripherals. Likewise, +3.3 V is supplied by the Arduino's FTIC chip and is limited to ~ 150 mA.

PlateFlo Python Package

The plateflo Python package, available from the Python Package Index (PyPI), includes several main modules: (1) fetbox, (2) scheduler, and a sub-package, (3) ismatec with modules for the Reglo Digital and Reglo ICC peristaltic pumps. Detailed API and usage documentation can be found at the project ReadTheDocs.

The fetbox module enables programmatic serial control of the FETbox hardware controller through a number of convenience functions. Each of the numbered MOSFET outputs can be switched on/off, output at a specific a PWM duty cycle, or use a type of switching optimized for solenoid valves called "hit-and-hold". The latter takes advantage of the fact that solenoid valves require far less power to maintain in the "on" position than they do during the initial switching operation. Full output power is supplied momentarily before reducing to a user specified PWM duty cycle. Using the hit-and-hold functionality reduces power draw and consequently heat generated by the solenoid coil. All of the Arduino's digital and analog input pins can also be read or written to via serial. Arbitrary strings can also be sent with either pass/fail or string responses for expanded functionality.

As the name implies, the scheduler module provides a means of creating tasks to be executed in the future. They can be set to execute at regular intervals, specific times, and scheduled tasks can be cancelled/removed from the scheduler at any time. Although intended as a companion to the fetbox module and ismatec sub-package, any callable Python object can be added to the scheduler with both keyword and positional arguments.

The ismatec sub-package has three modules: ismatec_scanner, ismatec_dig, and ismatec_icc. The ismatec_scanner is a utility for scanning system serial ports for attached Ismatec Reglo Digital and Reglo ICC peristaltic pumps. The ismatec_dig and ismatec_icc modules provide convenience functions for serial control of said pumps. These include starting/stopping, setting flowrate and direction, as well as querying current pump status, and printing messages on the pump's display. In the case of the Reglo ICC, individual pump channels can also be controlled.

Design files

All STL files are pre-oriented for FDM 3D printing. F3D and F3Z CAD files were created by Autodesk Fusion 360. PCB design source files, SCH & BRD, were created using Autodesk EAGLE [21]. Free education and hobbyist licenses are available for both Fusion 360 and EAGLE at the time of writing.

Design file name	File type	Open source license	Location
skimmer_clamp_M3	STL; CAD (F3Z); CAD (STEP)	CERN-OHL-W	https://doi.org/10.17605/OSF.IO/PYJCH
skimmer_height_block_<height > mm.stl	STL	CERN-OHL-W	https://doi.org/10.17605/OSF.IO/PYJCH
perfusion_lid_drill_jig	STL; CAD (STEP)	CERN-OHL-W	https://doi.org/10.17605/OSF.IO/PYJCH
petri_drill_jig_<size>_<inlet/outlet>	STL; CAD (STEP)	CERN-OHL-W	https://doi.org/10.17605/OSF.IO/PYJCH
valve_clip_base	STL; CAD (STEP)	CERN-OHL-W	https://doi.org/10.17605/OSF.IO/PYJCH
fetbox_complete	CAD (F3D); CAD (STEP)	CERN-OHL-W	https://doi.org/10.17605/OSF.IO/CRJVB

(*continued on next page*)

(*continued*)

Design file name	File type	Open source license	Location
fetbox_enclosure_base	STL	CERN-OHL-W	https://doi.org/10.17605/OSF.IO/CRJVB
fetbox_enclosure_lid	STL	CERN-OHL-W	https://doi.org/10.17605/OSF.IO/CRJVB
FETbox_rev0_Gerber_JLCPCB	Gerber CAM (ZIP folder)	CERN-OHL-W	https://doi.org/10.17605/OSF.IO/CRJVB
FETbox_rev0_PCB	EAGLE design file (SCH); EAGLE design file (BRD)	CERN-OHL-W	https://doi.org/10.17605/OSF.IO/CRJVB
Firmware_FETbox.ino	Firmware (INO)	CERN-OHL-W	https://doi.org/10.17605/OSF.IO/CRJVB
plateflo	Python package	GNU-GPL3+	PyPI; Source
Online Documentation	ReadTheDocs; Sphinx HTML	CC BY-SA 4.0	ReadTheDocs; https://osf.io/hev2z/
Supplementary Data	Folder	GNU-GPL3+	https://doi.org/10.17605/OSF.IO/PYJCH

- skimmer_clamp_M3 – Print-in-place skimmer nozzle clamping mechanism. Fixed atop a drilled Nunc OmniTray lid to allow precise positioning of the skimmer nozzle tip height. CAD files include modelled M3 fastener hardware as assembled.
- perfusion_lid_drill_jig – A guide for marking hole locations on Nunc OmniTray lids for drilling. Slides over top of the lid with holes for a fine-tipped marker.
- petri_drill_jig_<size>_<inlet/outlet> – As above, but for alternative petri dish culture chambers. Two pieces, inlet and outlet sides, that slide together to accommodate variability in petri dish dimension between manufacturers.
- valve_clip_base – Simple stand for the BOM pinch valve clip. Holds the valve horizontal for use on e.g. an incubator shelf.
- skimmer_height_block_<##>mm – Blocks of defined heights, <##>: 1.2, 1.4, 1.6, and 1.8 mm. Placed under the skimmer nozzle before tightening the skimmer clamp for repeatable height setting. Navigate to desired height model using left-side panel at listed OSF link.
- fetbox_complete - CAD model of the FETbox hardware controller with PCB and key electronic components modelled as assembled.
- fetbox_enclosure_base – the bottom half of the FETbox enclosure, into the which the PCB, power inlet, and MOSFET output jacks are mounted. adequate
- fetbox_enclosure_lid – the top cover of the FETbox enclosure. Has ventilation for the output MOSFETs and Arduino. It snap-fits onto the fetbox_enclosure_base.
- FETbox_rev0_Gerber_JLCPCB – Compressed (.zip) manufacturing Gerber (CAM) files. Ready for upload to the JLCPCB website for PCB ordering.
- FETbox_rev0_PCB – Autodesk EAGLE PCB source files for the FETbox_rev0_PCB. SCH and BRD files are co-dependent and must be downloaded together in order to open/modify the design.
- Firmware_FETbox – Arduino "sketch"/firmware for the Arduino Nano development board used in the FETbox hardware controller. Opened with Arduino IDE software.
- plateflo – A Python package containing modules to simplify coding serial control of the FETbox and Ismatec Reglo peristaltic pumps. See https://plateflo.readthedocs.io. for more details and usage.
- Online Documentation – searchable, mobile-friendly, companion documentation with sourcing guide, build guide, operating instructions, and programming examples.

Bill of materials

The tabulated bill of materials is available at https://plateflo.readthedocs.io/en/latest/hardware/bom.html as well as in Supplementary Data.

Required tools:

FDM 3D printer (e.g. Prusa MK3S) or 3D printing services
Small drill press, hand drill, or rotary tool (e.g. Dremel)
Cyanoacrylate (super) glue

Soldering iron (e.g. TS100)
Flux-core solder (e.g. Stannol Kristall 611)
Side cutters or similar (e.g. Knipex 78 61 125)
Hex wrench, 2.5 mm

Optional tools/components:

Isopropanol, 90%+ – for cleaning residual flux from PCB
Heat-shrink tubing – for DC input jack joint insulation
Self-adhesive silicone feet - for hardware controller and pinch valve stand

Build instructions

The PlateFlo system build is broken down into four distinct sections: 1) 3D printing & PCB ordering 2) FETbox assembly 3) perfusion plate modification/build. Detailed step-by-step instructions can be found in the project's online documentation (https://plateflo.readthedocs.io/en/latest/hardware/build_guide.html). See Supplementary Data "plateflo-readthedocs-v1.1.0.zip" for a downloadable copy of the online documentation.

Operating instructions

Operating instructions including setup guidelines, example configurations, skimmer pump operation, as well as plateflo package tutorials and API documentation can be found in the online documentation (https://plateflo.readthedocs.io/en/latest/hardware/operation.html). See Supplementary Data "plateflo-readthedocs-v1.1.0.zip" for a downloadable copy of the online documentation.

Validation and characterization

FETbox benchmarking & performance

Serial communication

Fidelity and maximum throughput of the serial communication protocol implemented in the FETbox firmware and plateflo serial input/output backend were verified using a stress test program. Arduino pin D3 was jumpered to pin D11. D3 was rapidly toggled HIGH/LOW with the state of D11 read after each D3 write command. The round-trip time of each write and read command, that is the elapsed time between starting to send the command and receiving the full response, was also measured for each cycle. This was repeated 10,000 times and logged to a data file (Supplementary Data, fetbox_serial_stresstest.csv). Failure to toggle the output state of D3 would result in an erroneous reading as the it would remain unchanged from the previous state, e.g. a low state when a high was commanded. Write commands were executed at 100% fidelity with zero discrepancies observed between the theoretical output of D3 and the read state of pin D11. Write and read commands were executed with round-trip times of 15.3 ± 1.3 ms and 16.0 ± 0.8 ms (mean ± St.Dev), respectively. For the digital write and read serial commands used here, a sustained command rate of 60–65 Hz can be expected. To validate these timing results, and to benchmark the round-trip time of other FETbox serial commands, a similar test was carried out without the overhead of input data collection. Using the timeit Python module, the time to successfully execute each command 50 consecutive times was measured. All commands measured 15.9 ms round-trip times with the exception of hit-and-hold which has an additional 100 ms delay built-in to allow time for the solenoid valve to engage (Supplementary Table 1). Utilizing a higher baud rate (115200 bps is the default) may enable slightly faster command rates at the risk of decreased reliability, especially when using longer cables.

PWM output

To characterize the MOSFET PWM output waveform, a Rigol DS1102Z-E oscilloscope was connected to FETbox output channel two at the MOSFET gate to measure the output from the Arduino as well as to the negative terminal of the flyback diode to measure the low-side output voltage to the connected device as in Fig. 3A,B. 10X probes limited to 20 MHz were used on both channels. The BOM pinch valve was connected to the FETbox output to serve as an inductive load. A PWM output value of 128 (~50% duty cycle) was set via serial command and the oscilloscope set to trigger on the rising edge of the Arduino PWM output at + 2.5 V (Fig. 3C). Rise time and fall time at the MOSFET gate were both determined to be ~ 250 ns (Fig S1A). This allows for PWM values from 5 (2% duty cycle) to 250 (98% duty cycle) to be used before static on or off states may occur (Fig S2). Flyback voltage spikes, which occur when an inductive load is disconnected during the off phase of the PWM signal, did not exceed 21 V at the highest PWM duty cycle (Fig S2), which is well within the 60 V drain-source voltage specification of the FQP30N06L MOSFET [22].

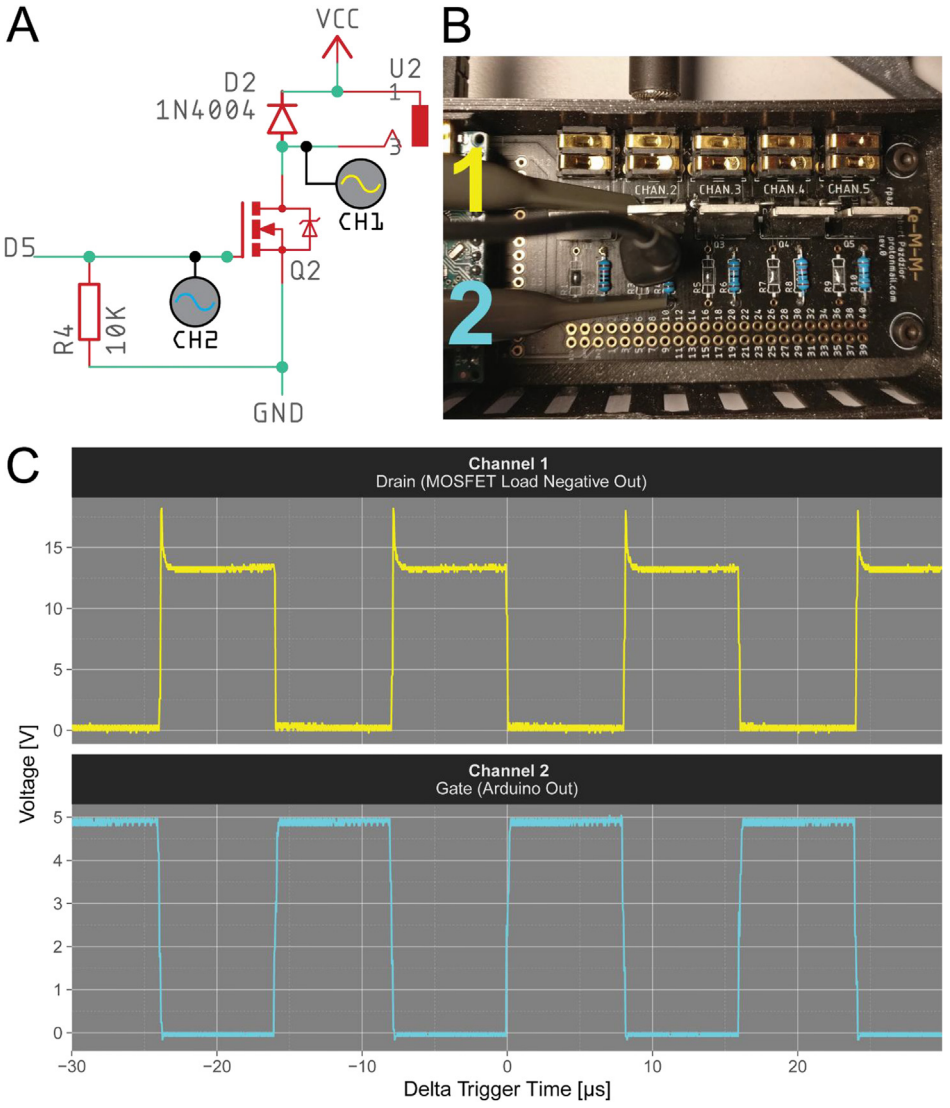

Fig. 3. FETbox Output Channel #2 PWM Waveform and Flyback Voltage Measurement. A) Schematic diagram of output channel #2 with oscilloscope probing points indicated by gray circles with colored waveform inside corresponding with oscilloscope channels 1 (yellow) and channel 2 (cyan) B) Image of probing setup. Grounding clip (black, middle) connected to ground side of the 10 K pulldown resistor, scope channel 1 to the MOSFET output low side, and scope channel 2 to the MOSFET gate to probe the Arduino PWM output. A pinch valve was plugged into the output to provide an inductive load. C) Oscilloscope traces during a 50% duty cycle PWM output. Note the carrier frequency period of 16 µs (62.5 kHz), and the freewheeling/flyback voltage spikes on the MOSFET output (yellow) less than 20 V. (For interpretation of the references to colour in this figure legend, the reader is referred to the web version of this article.)

Pinch valve mixing capability

With the exception of much more sophisticated proportional pinch valves, most pinch valves are binary devices, either fully engaged or fully disengaged. Arbitrary mixing ratios can, however, be achieved using the same principle that PWM uses to reduce effective output voltage from digital devices. Toggling the valve position for a fraction of a fixed time window will produce a mixture of the two inputs proportionally (Fig. 4B), provide that there is sufficient post-valve mixing. To validate mixing performance and assess the feasibility of programmable mixing profiles we used solutions of two different concentrations of glucose as a model (Fig. 4A). Two reservoirs of PBS solution, one containing 115 mg/dL (1 g/L nominal) and the other 210 mg/dL (2 g/L nominal) glucose (Fig. 4A) as measured using a Contour Next (Ascensia Diabetes Care) blood glucose meter and test strips, were connected to a pinch valve with a Y fitting. The pinch valve was set to mix the two channels according to the profile in Fig. 4D by varying the on/off duty cycle proportionally to the mixing ratio in two second windows, as illustrated in Fig. 4B. Pumping was handled by a Ismatec Reglo ICC 8-roller peristaltic pump (Cole-Parmer GmbH) at a calibrated flow rate of 250 µL/min. The flow was split after the peristaltic pump with another Y-piece and sampled at the

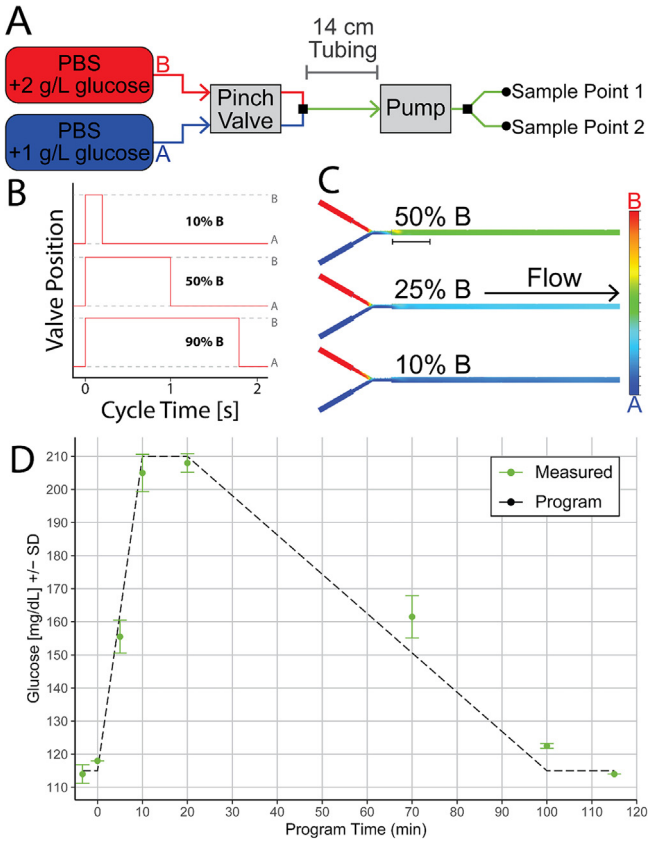

Fig. 4. Reservoir mixing performance evaluation. A) Experimental setup for mixing profile validation. Reservoirs of PBS containing 1–2 g/L were mixed programmatically via pinch valve into a Y-piece and quantified downstream simultaneously at two outlets. B) Illustrated pinch valve input mixing strategy, allows continuous mixing ratio output from discrete valve states. Mixing cycles loop continuously. C) CFD model cross-section of the discrete pinch valve mixing performance around the Y-piece fitting, approximating the region of (A) between the valve and pump. Colored by composition. Scale bar represents 10 mm. D) Programmed blood glucose concentration (dashed line) profile, emulating a post-prandial blood glucose spike in healthy adult human. Experimentally measured points are in green. (For interpretation of the references to colour in this figure legend, the reader is referred to the web version of this article.)

two outlets simultaneously using Contour Next (Ascensia Diabetes Care) blood glucose test strips. Total dead volume from valve to outlets (825 μL, ~3 min 20 s) was taken into consideration and sampling timing offset accordingly. The measured glucose profile followed the programmed profile closely, within the 10 mg/dL specified accuracy of the glucose meter (Fig. 4D).

A transient CFD simulation (Autodesk CFD 2019) was also constructed to study the mixing behavior in the pinch valve Y-piece fitting and downstream tubing. The fluid path of the junction was modeled using the measured 1 mm inner diameter and 60° angle of the Y-piece employed in the experimental setup and specified 1.52 mm inner diameter of the peristaltic tubing. A 10 mm segment of tubing was modelled for each input from the pinch valve and a single 140 mm segment of tubing for the output. A mean velocity of 2.296 mm/s in the tubing was calculated based on the 250 μL/min volumetric flow rate and tubing inner diameter used.

Static boundary conditions of 0 Pa pressure and 2.296 mm/s were applied to the outlet of the 140 mm tubing. Dynamic piecewise-linear boundary conditions for velocity were set at inlet tubing segments to mimic the discrete mixing behavior of the pinch valve in three different mixing ratio scenarios: 10%, 25%, and 50% B, where "B" indicates the 2 g/L glucose solution. E.g. at a 25% B mixing ratio, inlet B had a boundary condition of 2.296 mm/s for 0.5 s while A was at 0.0 mm/s, and then visa-versa for the remaining 1.5 s, repeating for the duration of the simulation. Scalar values of 0.0 (solution A) and 1.0 (solution B) were used to define the two glucose solutions with densities of 1.007 g/cm^3 and 1.0013 g/cm^3, respectively, with a scalar diffusion coefficient of 5.16e-06 mm^2/s and dynamic viscosity of 0.001100855 kg/m/s [23]. Initial conditions of scalar value 0.0 and 1.0 were defined in each of the inlet tubing volumes and scalar boundary conditions at the inlets were set accordingly. Turbulent incompressible flow physics were used, but similar results were obtained using laminar flow physics. Mesh sizing was done automatically, and no surface refinement was utilized. All other settings were kept at their default values.

Transient simulations were run for 120 s with 100 ms time-steps to fully capture the 10% mixing valve state duration (200 ms) and qualitative convergence was achieved before 70 s in all models. See Supplementary Video 1 for a real-time

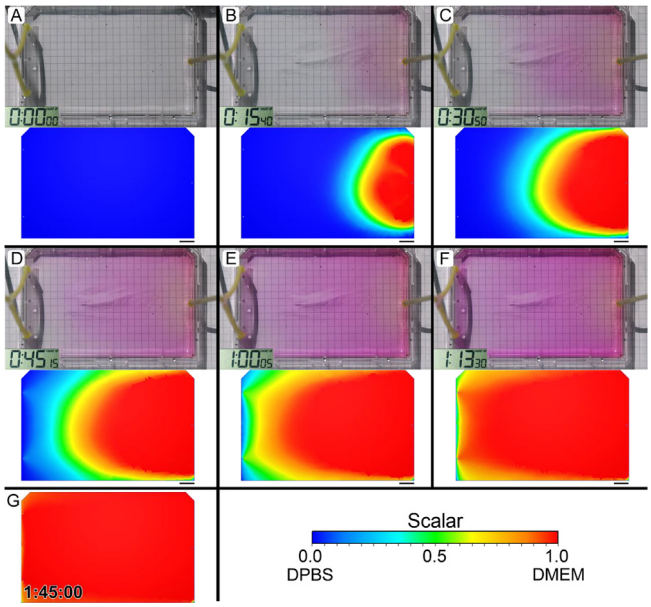

Fig. 5. Visualizing the flow profile of a PlateFlo culture plate. A-F) A plate preloaded with 10 mL of DPBS (colorless) was perfused with DMEM culture medium (pink) at 170 μL/min while a time lapse was recorded. Stopwatch inset in bottom left of each frame, h:mm:ss time format. A transient scalar mixing CFD model of plate flow at similar time intervals is also visualized below each time-lapse frame as an XY cross section the middle of the medium model. Black scale bar (bottom right, each panel) is 10 mm long. G) Transient model, as above, at 1 h 45 min. (For interpretation of the references to colour in this figure legend, the reader is referred to the web version of this article.)

visualization of the mixing behavior in the Y-piece for all ratios modelled, and Supplementary Video 2 with velocity vectors overlayed for the 50% mixing model. All components necessary to regenerate these data, including CAD model, mesh, and setup conditions can be found in the Autodesk CFD archive share file, y-piece_mixing_cfd.cfz, in Supplementary Data.

Scalar homogeneity near the target mixing ratio was achieved nearly immediately (less than10 mm) past the Y-piece fitting for all tested mixing ratios (Fig. 4C), indicating no need for additional mixing devices or tubing length.

Perfusion plate flow profiling

Part of the rationale for selecting OmniTray plates for the perfusion chamber was their rectangular aspect ratio. In order to keep fresh media flowing into the plate and spent media flowing out of it vortices and dead spots should be avoided.

We visualized the profile of flow across the plate by first loading a plate with 10 mL of colorless phosphate buffered saline (PBS) solution. The plate was then perfused with Dulbecco's Modified Eagle Medium (DMEM), a pink-colored solution of similar density, at 170 μL/min. A skimmer pump was not required for the short timescale of this experiment. A tripod mounted camera was used to photograph the plate from above at regular intervals and a lab timer was kept in the frame (lower left, photographs) for timekeeping purposes (Fig. 5A-F, upper). See Supplementary Video 3 for the full time-lapse video.

We also simulated this scenario using transient scalar mixing CFD modeling (Fig. 5A-F, lower; Fig. 5G), similar to as was conducted in 7.2. Fluid was modeled based on the dimensions of the plate and set to a height corresponding to 10 mL of volume. The P200 nozzles were modelled as 0.6 mm Ø cylindrical depressions from the top surface of the fluid extending down until 0.55 mm above the fluid bottom. Inlet and outlet boundary conditions were set at the lower surface of these depressions. Inlet boundary conditions included a developed volumetric flow rate of 170 μL/min and a scalar value of 0.0 until 1800 sec, then 1.0 for the remainder of the simulation. Outlet boundary conditions were 85 μL/min volumetric flow rate and 0 Pa pressure. Fluid properties were defined identically to that in section 7.2, approximating culture medium. A steady-state solution was first solved for the velocity (~100 iterations), then a transient solution was found for scalar mixing to visualize the flow profile across the plate up until 8600 s. Simulation results are illustrated using a cross sections along the XY plane, through the middle of the media model and colored according to the scalar mixing ratio of 0.0–1.0 (PBS-DMEM) in Fig. 5A-F, lower and Fig. 5G. See Supplementary Video 4 for the complete simulation animation, and Supplementary Data for the Autodesk CFD archive share file, plateflo_perfusion_plate_CFD.cfz, to reproduce the model results.

The time required for the DMEM front to traverse the plate was approximately 73 min. Experimental and simulation flow profiles appeared similar. Both showed mixing of the DMEM front as it progressed across the plate, becoming more diffuse towards the outlet side. The chamfered corners of the OmniTray plate (upper left, upper right) appear to improve flow linearity when compared with the orthogonal opposing corners (lower left, lower right) which show some flow stagnation as indicated by the lower scalar value towards the end of the time series. Although not entirely homogenous, the vast majority

of cells seeded onto a perfusion plate are subject to similar microenvironmental conditions as culture medium moves consistently across the plate's surface, with negligible dead spots.

Discussion

Areas for Improvement

Perfusion plate skimmer system

The skimming approach we've taken to plate volume regulation, though relatively simple and cost-effective, is negatively influenced by surface tension and capillary action. Fluid cannot be aspirated unless it contacts the skimmer nozzle. Once the fluid comes into contact with the skimmer nozzle it is drawn up into the bore. As material is removed the fluid level drops. Surface tension, however, maintains an unbroken column of fluid stretched between the nozzle and the bulk fluid, bridging the fluid surface and the nozzle, and permitting continued removal of material from the plate despite the fluid level dropping below the level of the nozzle. The stretches as the level drops until it eventually breaks, at which point the fluid surface is below the level of the skimmer nozzle. Fluid then slowly accumulates until it contacts the skimmer nozzle and the cycle continues. In this way an approximately saw tooth shaped oscillation in fluid volume is created in the plate, the frequency of which is dependent on the inlet/outlet flow rate delta, i.e. faster accumulation results in a higher oscillation rate. For this reason, it is recommended that the flow rate delta be kept as small as possible. Nozzle geometry could potentially be better optimized to minimize this phenomenon [24]. Optimized skimmer geometry would, however, likely come at the expense of additional cost and build/sourcing complexity.

FETbox hardware controller

In the interest of minimizing BOM component count and PCB assembly complexity, a dedicated DC-DC conversion circuit was not implemented on the FETbox board. Instead, the 12 V supply voltage is converted to 5 V and 3.3 V through the Arduino Nano's onboard regulators. Though 12 V is within specification for the input voltage, it is on the upper end of the acceptable range. As such the Nano's linear voltage regulators generate a lot of heat. Drawing additional current from the 5 V line for additional components (status LCD, or LEDs for example) further increases heat output. This could be addressed with a buck converter module such as a Würth Elektronik 173950578 [25], or a suitable dedicated daughter board for higher-current 5 V applications. This would supply the Nano via the 5 V pin, rather than the Vin pin due to the dropout voltage across the Vin regulator circuitry.

If the FETbox is connected by USB and not powered from the 12 V input (e.g. by accidental disconnection) and the MOSFET outputs are engaged, the connected output devices will draw from the Vin pin which in this instance will be connected directly to the USB port 5 V bus. To avoid this, an additional 1 N4004 power diode can be placed between the power input and Vin pin, preventing current from flowing out from the Arduino and keeping the MOSFET output unpowered. Placing a diode in front of the Nano Vin pin has the added benefit of dropping the input voltage by 1 V, reducing the heat output from the Nano's onboard regulators.

Potential applications

The programmability of the PlateFlo system lends itself to dynamic culture protocols where culture conditions are regimented, vary over time in a controlled manner. Certain embryonic stem cell expansion and differentiation protocols, for example, involve a series of culture media changes and/or compound doses to affect developmental progress [26]. In addition to specific molecular cues, numerous studies have demonstrated osteogenic differentiation of mesenchymal stem cells also benefits from biophysical cues in the form of shear stress [27,28]. For example, the perfusion system presented by Pasini et al, which is similar in principle to that of the PlateFlo system, demonstrates improved induction of osteogenic gene expression under flow when compared with induction in static culture [20]. Even very low flow, such as that experienced in interstitial fluid can induce osteogenic differentiation [29,30]. Oscillating fluid shear has also been shown to benefit osteoblast differentiation to a greater extent than continuous perfusion alone [31], and could easily be implemented in the perfusion plate using computer controlled peristaltic pumps such as with the ismatec sub-package in the plateFlo Python library. These protocols could potentially benefit from partial or complete integration into the PlateFlo system but require validation on a case-by-case basis. Flow rate and plate volume can be adjusted to increase or decrease shear stress across the culture surface. For a given volumetric flow rate, a greater plate volume will result in lower linear velocity and therefore lower shear forces. This will result in a lower rate of exchange and therefore greater accumulation of secreted factors and potential for local or even global nutrient depletion. Skimmer height can be set using the various printed skimmer height blocks. See "Operating Instructions" for more details.

In order to maintain pluripotency and stimulate growth, embryonic stem cells (ESCs) are often co-cultured on a layer of "feeder" cells, mouse embryonic fibroblasts [32] or human embryonic stem cells [33], that supply a complex mixture of factors to the ESC. Although strides have been made towards feeder-free expansion and differentiation [34–36], not all ESC lines or differentiation protocols may be amenable to this approach. By adapting the PlateFlo setup showcased in the graphical abstract, for example, it may be possible to co-culture feeder and some ESC lines in physically isolated plates. This has

the potential to simplify downstream processing while benefiting from a constant flow of fresh medium. When expanding embryonic stem cells, waste products such as lactic acid and ammonia can accumulate and limit cell viability in non-perfused systems [37]. Recirculating media however, either partially or fully, may be more economical in certain scenarios given the high cost of ESC culture medium and supplements. This application has not been validated but we believe it to be an interesting avenue for future exploration. Many other biological applications that rely on the use of conditioned media should also benefit from the PlateFlo setup. In all cases, flow rate and plate volume would be the main parameters to adjust. This could be done for each plate individually to e.g. concentrate the secreted factors using a lower plate volume upstream while maintaining the downstream plate at a higher volume for slower exchange.

Alternative culture chambers

The OmniTray was selected early on in the conceptualization of the PlateFlo system for its rectangular shape. Theoretically this yields the most consistent flow across the plate as it minimizes the difference between the longest and shortest path media could take from inlet to outlet. The OmniTray also has a standard footprint that is directly compatible with e.g. plate holders in automated microscopes and is available with a treated culture surface at a price of ca. 10EUR/plate, making it a relatively affordable option. It is, however, a single-source item and therefore susceptible to discontinuation, supply chain disruption, and price hikes.

Nunc offers a four well plate in the same footprint with rectangular wells that each fit a 75 $\times$ 25 mm glass slide (ThermoFisher Scientific, cat# 267061). This plate format could be of use when lower flow rates and media consumption are desirable, or material is limited as with e.g. primary tissues. Reducing the volume while maintaining a similar flow rate would also increase the media exchange rate and linear velocity of the fluid. The lack of a treated surface version creates additional preparation steps for use with adherent cells, however. One potential work around would be to use treated slides (e.g ThermoScientific, cat# 960004) as drop-in culture surfaces. For some applications, non-treated surfaces might be preferred, as in the case of primary pancreatic islet culture. We successfully carried out a pilot experiment with primary pancreatic islets in one of these untreated wells, without noticeable movement of the islets with flow. This format is interesting as a smaller alternative with similar geometry but requires further validation and unfortunately is also a single-source item.

Petri dishes are ubiquitous and available in a range of sizes from many suppliers and manufacturers. The general linear flow characteristics of circular dishes are not as favorable as those of rectangular form factor plates such as the OmniTray (Supplementary Fig. 3). A CFD simulation of particles (representing paths of flow) moving across a 10 cm petri dish (similar in culture area to an OmniTray plate) showed a wider distribution of residence times when compared with the OmniTray (standard deviation 660 s vs 530 s) (Supplementary Fig. 3D). However, their availability, low cost, and range of sizes make them an attractive future-proof alternative to the Nunc OmniTray. As such, we've included design files for 3D printing nozzle hole marking jigs for 6 cm, 10 cm, and 15 cm petri dish lids. These jigs feature a two-part sliding design that allows the jig to adapt to small dimensional variation in petri dish lids between the various manufacturers. We have not validated the use of petri dishes for perfusion experimentally, however, CFD simulations suggest an acceptable flow profile in 10 cm plates.

Integration with open source tools

A commercial multi-channel peristaltic pump is listed in the PlateFlo BOM, the Ismatec Reglo ICC. This is primarily for its flexibility, having individually controllable channels enabling two-plate multiplexing while being able to run with the inlet/outlet flow rate delta required, all in a single unit. Though well-suited to the PlateFlo system, and easily re-configured for different setups, the cost of a single 4-channel unit is extremely high (list price 3600EUR at time of writing). A viable open source alternative could quite easily, for example, make use of a pair of FAST [38] 3D-printed peristaltic pumps, each of which could be controlled via USB from the same computer that interfaces with the FETbox hardware controller. This would also allow a larger number of perfusion plates to be run in parallel than e.g. a single Reglo ICC pump.

A potentially interesting addition to the PlateFlo system which may be of interest in the study of e.g. endocrine culture models, is a downstream sampler for automated supernatant sample collection. The recent BioSamplr [39] system could, for example, be integrated downstream of the PlateFlo system with some minor modifications. An additional dual-channel pinch valve (as in e.g. the BOM) can be placed in the PlateFlo outlet tubing path and used to create sample loop (as in HPLC injectors, for example), allowing the BioSamplr's peristaltic pump to pull supernatant from this section of tubing when engaged, and bypassing it when disengaged (Supplementary Fig. 4). The PlateFlo outlet peristaltic pump should be temporarily disabled during sampling, as the outlet will be blocked by the pinch valve when engaged. Integration of the PlateFlo and BioSamplr Python software would permit complete automated control of both systems from the BioSamplr's Raspberry Pi computer, removing the need for an additional control computer for the FETbox.

Declaration of Competing Interest

The authors declare no conflicts of interest. R.P. gratefully acknowledges support by a DOC PhD Fellowship of the Austrian Academy of Sciences. Research in the Kubicek lab is supported by the Austrian Federal Ministry for Digital and Economic Affairs and the National Foundation for Research, Technology, and Development, the Austrian Science Fund (FWF) F4701

and the European Research Council (ERC) under the European Union's Horizon 2020 research and innovation programme (ERC-CoG-772437).

Appendix A. Supplementary data

Supplementary data to this article can be found online at https://doi.org/10.1016/j.ohx.2021.e00222.

References

[1] J.R. Masters, G.N. Stacey, Changing medium and passaging cell lines, Nat. Protoc. 2 (9) (2007) 2276–2284, https://doi.org/10.1038/nprot.2007.319.
[2] Anton G. Kutikhin, Maxim Yu. Sinitsky, Arseniy E. Yuzhalin, Elena A. Velikanova, Shear stress: An essential driver of endothelial progenitor cells, Journal of Molecular and Cellular Cardiology 118 (2018) 46–69, https://doi.org/10.1016/j.yjmcc.2018.03.007.
[3] Q. Ma, Z. Ma, M. Liang, F. Luo, J. Xu, C.e. Dou, S. Dong, The role of physical forces in osteoclastogenesis, J. Cell. Physiol. 234 (8) (2019) 12498–12507, https://doi.org/10.1002/jcp.28108.
[4] Z. Li, Z. Cui, Three-dimensional perfused cell culture, Biotechnol. Adv. 32 (2) (2014) 243–254, https://doi.org/10.1016/j.biotechadv.2013.10.006.
[5] V. Starokozhko, M. Hemmingsen, L. Larsen, S. Mohanty, M. Merema, R.C. Pimentel, A. Wolff, J. Emnéus, A. Aspegren, G. Groothuis, M. Dufva, Differentiation of human-induced pluripotent stem cell under flow conditions to mature hepatocytes for liver tissue engineering, J. Tissue Eng. Regen. Med. 12 (5) (2018) 1273–1284.
[6] D. Bulnes-Abundis, L.M. Carrillo-Cocom, D. Aráiz-Hernández, A. García-Ulloa, M. Granados-Pastor, P.B. Sánchez-Arreola, G. Murugappan, M.M. Alvarez, A simple eccentric stirred tank mini-bioreactor: Mixing characterization and mammalian cell culture experiments, Biotechnol. Bioeng. 110 (4) (2013) 1106–1118.
[7] D.E. Discher, Tissue Cells Feel and Respond to the Stiffness of Their Substrate, Science 310 (5751) (2005) 1139–1143.
[8] A.L. Van Wezel, Growth of Cell-strains and Primary Cells on Micro-carriers in Homogeneous Culture, Nature 216 (5110) (1967) 64–65, https://doi.org/10.1038/216064a0.
[9] B. Nankervis, M. Jones, B. Vang, R. Brent Rice Jr, C. Coeshott, J. Beltzer, Optimizing T Cell Expansion in a Hollow-Fiber Bioreactor, Curr. Stem Cell Rep. 4 (1) (2018) 46–51, https://doi.org/10.1007/s40778-018-0116-x.
[10] R.A. Knazek, P.M. Gullino, P.O. Kohler, R.L. Dedrick, Cell Culture on Artificial Capillaries: An Approach to Tissue Growth in vitro, Science 178 (4056) (1972) 65–67.
[11] J.B. Dahl, J.-M. Lin, S.J. Muller, S. Kumar, Microfluidic Strategies for Understanding the Mechanics of Cells and Cell-Mimetic Systems, Annu. Rev. Chem. Biomol. Eng. 6 (1) (2015) 293–317.
[12] A. Essaouiba, T. Okitsu, R. Jellali, M. Shinohara, M. Danoy, Y. Tauran, C. Legallais, Y. Sakai, E. Leclerc, Microwell-based pancreas-on-chip model enhances genes expression and functionality of rat islets of Langerhans, Mol. Cell. Endocrinol. 514 (2020) 110892, https://doi.org/10.1016/j.mce:2020.110892.
[13] E. Behroodi, H. Latifi, Z. Bagheri, E. Ermis, S. Roshani, M. Salehi Moghaddam, A combined 3D printing/CNC micro-milling method to fabricate a large-scale microfluidic device with the small size 3D architectures: an application for tumor spheroid production, Sci. Rep. 10 (1) (2020), https://doi.org/10.1038/s41598-020-79015-5.
[14] T. Schulze et al, A Parallel Perifusion Slide From Glass for the Functional and Morphological Analysis of Pancreatic Islets, Front. Bioeng. Biotechnol. 9 (2021), https://doi.org/10.3389/fbioe.2021.615639.
[15] M. G. Moretti, L. E. Freed, and R. S. Langer, 'Oscillating cell culture bioreactor', US20100297233A1, Nov. 25, 2010 Accessed: Jul. 19, 2021. [Online]. Available: https://patents.google.com/patent/US20100297233A1/en
[16] M. G. Moretti, L. E. Freed, and R. S. Langer, 'Oscillating cell culture bioreactor', US9217129B2, Dec. 22, 2015 Accessed: Jul. 19, 2021. [Online]. Available: https://patents.google.com/patent/US9217129B2/en
[17] R. Visone, G. Talò, S. Lopa, M. Rasponi, M. Moretti, Enhancing all-in-one bioreactors by combining interstitial perfusion, electrical stimulation, on-line monitoring and testing within a single chamber for cardiac constructs, Sci. Rep. 8 (1) (Nov. 2018) 16944, https://doi.org/10.1038/s41598-018-35019-w.
[18] Y. Abe et al, Improved phosphoproteomic analysis for phosphosignaling and active-kinome profiling in Matrigel-embedded spheroids and patient-derived organoids, Sci. Rep. 8 (1) (Jul. 2018) 11401, https://doi.org/10.1038/s41598-018-29837-1.
[19] K. Domansky, W. Inman, J. Serdy, A. Dash, M.H.M. Lim, L.G. Griffith, Perfused multiwell plate for 3D liver tissue engineering, Lab. Chip 10 (1) (Jan. 2010) 51–58, https://doi.org/10.1039/B913221J.
[20] A. Pasini, J. Lovecchio, G. Ferretti, E. Giordano, Medium Perfusion Flow Improves Osteogenic Commitment of Human Stromal Cells, Stem Cells Int. 2019 (2019), https://doi.org/10.1155/2019/1304194 e1304194.
[21] 'EAGLE | PCB Design And Electrical Schematic Software | Autodesk'. https://www.autodesk.com/products/eagle/overview, (accessed Dec. 16, 2020).
[22] Fairchild Semiconductor, 'FQP30N06L - N-Channel QFET MOSFET Datasheet'. Mouser, Nov. 01, 2013, Accessed: Mar. 10, 2021. [Online]. Available: https://eu.mouser.com/datasheet/2/308/FQP30N06L-D-1809681.pdf.
[23] H. Suhaimi, S. Wang, D.B. Das, Glucose diffusivity in cell culture medium, Chem. Eng. J. 269 (2015) 323–327, https://doi.org/10.1016/j.cej.2015.01.130.
[24] J. Molenaar, W.G.N. van Heugten, C.J.M. van Rijn, Viscous Liquid Threads with Inner Fluid Flow Inside Microchannels, ACS Omega 4 (6) (2019) 9800–9806.
[25] Würth Elektronik, 'MagI3C Power Module Datasheet'. Digikey, May 01, 2019, Accessed: Mar. 11, 2021. [Online]. Available: https://media.digikey.com/pdf/Data%20Sheets/Wurth%20Electronics%20PDFs/173950378_173950578.pdf.
[26] Y. Shi, P. Kirwan, F.J. Livesey, Directed differentiation of human pluripotent stem cells to cerebral cortex neurons and neural networks, Nat. Protoc. 7 (10) (2012) 1836–1846, https://doi.org/10.1038/nprot.2012.116.
[27] M.D. Aisha, M.N.K. Nor-Ashikin, A.B.R. Sharaniza, H. Nawawi, G.R.A. Froemming, Orbital fluid shear stress promotes osteoblast metabolism, proliferation and alkaline phosphates activity in vitro, Exp. Cell Res. 337 (1) (2015) 87–93, https://doi.org/10.1016/j.yexcr.2015.07.002.
[28] Z. Bo, G. Bin, W. Jing, W. Cuifang, A.n. Liping, M.a. Jinglin, J. Jin, T. Xiaoyi, C. Cong, D. Ning, X. Yayi, Fluid shear stress promotes osteoblast proliferation via the Gαq–ERK5 signaling pathway, Connect. Tissue Res. 57 (4) (2016) 299–306.
[29] K.M. Kim et al, Shear stress induced by an interstitial level of slow flow increases the osteogenic differentiation of mesenchymal stem cells through TAZ activation, PLoS One 9 (3) (2014) e92427, https://doi.org/10.1371/journal.pone.0092427.
[30] U.M. Liegibel et al, Fluid shear of low magnitude increases growth and expression of TGFbeta1 and adhesion molecules in human bone cells in vitro', Exp. Clin. Endocrinol. Diabetes Off. J. Ger. Soc. Endocrinol. Ger. Diabetes Assoc. 112 (7) (2004) 356–363, https://doi.org/10.1055/s-2004-821014.
[31] P. Li, Y.-C. Ma, X.-Y. Sheng, H.-T. Dong, H. Han, J. Wang, Y.-y. Xia, Cyclic fluid shear stress promotes osteoblastic cells proliferation through ERK5 signaling pathway, Mol. Cell. Biochem. 364 (1-2) (2012) 321–327, https://doi.org/10.1007/s11010-012-1233-y.
[32] J.A. Thomson et al, Embryonic Stem Cell Lines Derived from Human Blastocysts, Science 282 (5391) (Nov. 1998) 1145–1147, https://doi.org/10.1126/science.282.5391.1145.
[33] M. Richards, C.-Y. Fong, W.-K. Chan, P.-C. Wong, A. Bongso, Human feeders support prolonged undifferentiated growth of human inner cell masses and embryonic stem cells, Nat. Biotechnol. 20 (9) (2002) 933–936, https://doi.org/10.1038/nbt726.
[34] I. Chatterjee, F. Li, E.E. Kohler, J. Rehman, A.B. Malik, K.K. Wary, Induced Pluripotent Stem (iPS) Cell Culture Methods and Induction of Differentiation into Endothelial Cells, Methods Mol. Biol. Clifton NJ 1357 (2016) 311–327, https://doi.org/10.1007/7651_2015_203.

[35] H. Zhu, D.S. Kaufman, An Improved Method to Produce Clinical-Scale Natural Killer Cells from Human Pluripotent Stem Cells, Methods Mol. Biol. Clifton NJ 2048 (2019) 107–119, https://doi.org/10.1007/978-1-4939-9728-2_12.
[36] J. Dahlmann et al, Generation of functional cardiomyocytes from rat embryonic and induced pluripotent stem cells using feeder-free expansion and differentiation in suspension culture, PLoS One 13 (3) (2018) e0192652, https://doi.org/10.1371/journal.pone.0192652.
[37] J.T. Cormier, N.I.Z. Nieden, D.E. Rancourt, M.S. Kallos, Expansion of Undifferentiated Murine Embryonic Stem Cells as Aggregates in Suspension Culture Bioreactors, Tissue Eng. 12 (11) (2006) 3233–3245.
[38] A. Jönsson, A. Toppi, M. Dufva, The FAST Pump, a low-cost, easy to fabricate, SLA-3D-printed peristaltic pump for multi-channel systems in any lab, HardwareX 8 (2020) e00115, https://doi.org/10.1016/j.ohx.2020.e00115.
[39] J.P. Efromson, S. Li, M.D. Lynch, BioSamplr: An open source, low cost automated sampling system for bioreactors, HardwareX 9 (2021) e00177, https://doi.org/10.1016/j.ohx.2021.e00177.
[40] G. Talò et al, Industrialization of a perfusion bioreactor: Prime example of a non-straightforward process, J. Tissue Eng. Regen. Med. 12 (2) (2018) 405–415, https://doi.org/10.1002/term.2480.
[41] B.F.L. Lai et al, A well plate–based multiplexed platform for incorporation of organoids into an organ-on-a-chip system with a perfusable vasculature, Nat. Protoc. 16 (4) (Apr. 2021) 2158–2189, https://doi.org/10.1038/s41596-020-00490-1.
[42] M.S. Mousavi, G. Amoabediny, S.H. Mahfouzi, S.H. Safiabadi Tali, Enhanced articular cartilage decellularization using a novel perfusion-based bioreactor method, J. Mech. Behav. Biomed. Mater. 119 (Jul. 2021) 104511, https://doi.org/10.1016/j.jmbbm.2021.104511.
[43] C. Manfredonia et al, Maintenance of Primary Human Colorectal Cancer Microenvironment Using a Perfusion Bioreactor-Based 3D Culture System, Adv. Biosyst. 3 (4) (2019) 1800300, https://doi.org/10.1002/adbi.201800300.
[44] C. Hirt et al, Bioreactor-engineered cancer tissue-like structures mimic phenotypes, gene expression profiles and drug resistance patterns observed in vivo, Biomaterials 62 (2015) 138–146, https://doi.org/10.1016/j.biomaterials.2015.05.037.
[45] M. Bartnikowski, T.J. Klein, F.P.W. Melchels, M.A. Woodruff, Effects of scaffold architecture on mechanical characteristics and osteoblast response to static and perfusion bioreactor cultures, Biotechnol. Bioeng. 111 (7) (2014) 1440–1451, https://doi.org/10.1002/bit.25200.
[46] I.E. Chesnick, F.A. Avallone, R.D. Leapman, W.J. Landis, N. Eidelman, K. Potter, Evaluation of bioreactor-cultivated bone by magnetic resonance microscopy and FTIR microspectroscopy, Bone 40 (4) (Apr. 2007) 904–912, https://doi.org/10.1016/j.bone.2006.10.020.
[47] I.J. Jayaprakash, N.S. Jayaprakash, Trends in Monoclonal Antibody Production Using Various Bioreactor Systems 31 (3) (Mar. 2021) 349–357, https://doi.org/10.4014/jmb.1911.11066.
[48] H. Morschett et al, Robotic integration enables autonomous operation of laboratory scale stirred tank bioreactors with model-driven process analysis, Biotechnol. Bioeng. 118 (7) (2021) 2759–2769, https://doi.org/10.1002/bit.27795.
[49] Isidro I. A., et al., Online monitoring of hiPSC expansion and hepatic differentiation in 3D culture by dielectric spectroscopy, Biotechnol. Bioeng., doi:10.1002/bit.27751.

Robert Pazdzior is a Canadian citizen born 1993 in Canada. He began studies in Biochemistry & Molecular at Trent University (Peterborough, ON, Canada) in 2011, where he first gained research experience and an interest in research under the supervision of Steven Rafferty through three Natural Sciences and Engineering Research Council of Canada (NSERC) Undergraduate Research awards. He graduated from Trent on the President's Honour Roll in 2015. Following entry into the CeMM PhD program in Vienna, Austria, he then joined the Kubicek lab where he was awarded the Austrian Academy of Sciences DOC PhD fellowship and developed a keen interest in 3D printing, 3D design, mechatronics, and programming during his PhD thesis work on pancreatic α- and β-cell biology and tissue culture models.

Stefan Kubicek, PhD., is an Austrian citizen born 1978 in Vienna. He studied synthetic organic chemistry at the Vienna University of Technology and the Swiss Federal Institute of Technology (with François Diederich, ETH Zürich). For his PhD in Molecular Biology he developed the first specific histone methyltransferase inhibitor at the Institute of Molecular Pathology IMP Vienna (advisor Thomas Jenuwein). He then spent 3 years as a postdoctoral fellow at the Broad Institute of Harvard and MIT in Cambridge, MA, USA (Chemical Biology Program, Stuart Schreiber laboratory). Since 2010 he heads the Platform Austria for Chemical Biology PLACEBO at CeMM. Since 2013 he headed the Christian Doppler laboratory for Chemical Epigenetics and Antiinfectives, a public-private partnership between CeMM, Boehringer Ingelheim, and Haplogen. Since 2017 he heads the Proteomics and Metabolomics Facility at CeMM. Research in the Kubicek lab is funded by the Austrian Academy of Sciences, the European Research Council ERC, the Juvenile Diabetes Research Foundation JDRF, the Austrian Federal Ministry of Science, Research and Economy and the National Foundation for Research, Technology, and Development, and the Austrian Science Fund FWF. Stefan Kubicek studies chromatin, epigenetics and small molecules that change cell fates in oncology and diabetes with a particular focus on metabolism in the cell's nucleus.